Science and Technology for the Built Environment

ISSN: 2374-4731 (Print) 2374-474X (Online) Journal homepage: http://www.tandfonline.com/loi/uhvc21

Design of a hydraulically driven compressive elastocaloric cooling system

Suxin Qian, Yunlong Geng, Yi Wang, Jan Muehlbauer, Jiazhen Ling, Yunho Hwang, Reinhard Radermacher & Ichiro Takeuchi

To cite this article: Suxin Qian, Yunlong Geng, Yi Wang, Jan Muehlbauer, Jiazhen Ling, Yunho Hwang, Reinhard Radermacher & Ichiro Takeuchi (2016): Design of a hydraulically driven compressive elastocaloric cooling system, Science and Technology for the Built Environment, DOI: 10.1080/23744731.2016.1171630

To link to this article: http://dx.doi.org/10.1080/23744731.2016.1171630

Accepted author version posted online: 30 Mar 2016.
Published online: 30 Mar 2016.

Science and Technology for the Built Environment (2016) **00**, 1–7

ISSN: 2374-4731 print / 2374-474X online
DOI: 10.1080/23744731.2016.1171630

Taylor & Francis
Taylor & Francis Group

Design of a hydraulically driven compressive elastocaloric cooling system

SUXIN QIAN[1,2], YUNLONG GENG[3], YI WANG[3], JAN MUEHLBAUER[2], JIAZHEN LING[2], YUNHO HWANG[2,*], REINHARD RADERMACHER[2], and ICHIRO TAKEUCHI[3]

[1]*Department of Refrigeration and Cryogenic Engineering, School of Energy and Power Engineering, Xi'an Jiaotong University, China*
[2]*Department of Mechanical Engineering, University of Maryland, College Park, 3157 Glenn L. Martin Hall, College Park, MD 20742, USA*
[3]*Department of Materials Science and Engineering, University of Maryland, College Park, MD, USA*

This article presents the design of elastocaloric cooling system driven by hydraulic actuators. Ni-Ti tubes under axial compressive loading mode are used in the system to provide cooling and heating. Those Ni-Ti tubes are enclosed in four identical beds, which are driven by two one-way hydraulic cylinders. Operated under the single-stage reverse Brayton cycle, the system achieves heat transfer and heat recovery by using a sophisticated heat transfer fluid network controlled by solenoid valves. Two novel designs to improve the system's performance based on the lessons learned from the previous studies are applied to this prototype. Preliminary test results of the material's latent heat at a specific fluid flow rate and temperature difference agree well with the results reported in the literature. System coefficient of performance of 11.0 and temperature lift of 24.6 K are estimated based on a dynamic model developed in the previous study.

Introduction

Elastocaloric cooling is an up-and-coming new solid-state cooling technology using shape memory alloys (SMAs) as refrigerants. Heating or cooling can be generated by phase transformation between the solid-state austenite phase and martensite phase in SMAs (Otsuka and Wayman 1998). The phase transformation in a cooling system is induced by applied stress. Upon loading of stress, the anstenite phase transforms to martensite phase while releasing latent heat. Removal of the stress corresponds to the cooling process during the reverse phase change. The major interest of investigating this new solid-state cooling technology is to eliminate the use of conventional refrigerants with a large global warming potential, as well as improving the energy efficiency of traditional vapor compression cooling systems (Manosa et al. 2009). Comprehensive reviews of the current state-of-the-art of elastocaloric cooling can be found in Qian et al. (2016a) and Kitanovski et al. (2015). Compared with other competitive novel solid state cooling technologies, such as magnetocaloric cooling (Jacob et al. 2014) and electrocaloric cooling (Ozbolt et al. 2014), elastocaloric cooling has the largest latent heat and energy storage density (Qian et al. 2016b), which is attractive since materials with less weight and lower cost are needed to meet the same cooling demand. It also opens more possibilities in cycle choice and system integration, since a single-stage cycle using SMAs may be enough for some applications instead of a complicated cascaded cycle design (Tusek et al. 2015a).

Such a single-stage cycle can be achieved by a reverse Brayton cycle, as illustrated in Figure 1 (Qian et al. 2015a). Two beds of SMA are required to provide continuous cooling, wherein those two beds have a delay of half a cycle. The cycle starts by applying stress to the first bed from state 1 to state 2 adiabatically, and releasing the stress in the second bed from state 4 to state 5. Followed by the heat transfer process, the first bed rejects heat to the heat sink (T_h) and the second bed absorbs heat from the heat source (T_c). The cycle completes by an internal heat recovery (HR) process driven by the temperature difference between the two beds, to precool the first bed from state 3 to state 4 and preheat the second one from state 6 back to state 1. The loading process may be driven by uniaxial compression or tension. It was pointed out that a cycle under compression is more efficient than one under tension due to a lower material level hysteresis (Cui et al. 2012). Multiple single-stage cycles could form a cascaded system to

Received December 15, 2015; accepted February 24, 2016
Suxin Qian, PhD, is an Assistant Professor. **Yunlong Geng, PhD,** is a Postdoctoral Scholar. **Yi Wang, PhD,** is a Postdoctoral Scholar. **Jan Muehlbauer, MS,** is a Faculty Research Associate. **Jiazhen Ling, PhD,** Affiliate Member ASHRAE, is a Research Assistant Professor. **Yunho Hwang, PhD,** Member ASHRAE, is a Research Professor. **Reinhard Radermacher, PhD,** Fellow ASHRAE, is a Minta Martin Professor. **Ichiro Takeuchi, PhD,** is a Professor.
*Corresponding author e-mail: yhhwang@umd.edu
Color versions of one or more of the figures in the article can be found online at www.tandfonline.com/uhvc.

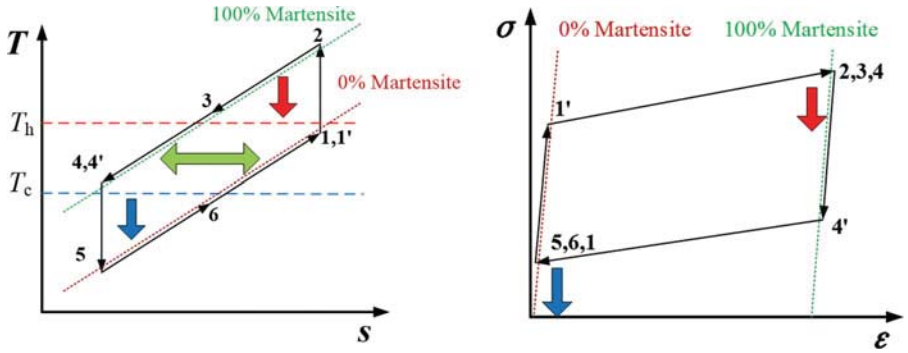

Fig. 1. Illustration of a single-stage Brayton cycle using SMAs.

achieve a higher system temperature lift. A cascaded cycle with simultaneous heat transfer and HR can be achieved by the so-called active regenerator design, which has been used in magnetocaloric cooling systems for decades (Tusek et al. 2015a).

The previously mentioned single-stage cycle and its simpler modifications were used in previous studies. Qian et al. (2015b) developed the world's first of-its-kind prototype using Ni-Ti tubes under compression with water as the heat transfer fluid (HTF). HR was enabled by an internal water loop, which was optimized based on a systematic design study (Qian et al. 2015b). The maximum water–water temperature lift achieved was 4.7 K and the maximum cooling capacity was 65 W. Whereas, Schmidt et al. (2014 2015) developed an elastocaloric cooling device using Ni-Ti ribbon under tensile without a HTF. The cyclic heat transfer between the SMA bed and heat sources was achieved by two motive solid pieces controlled by linear motors, wherein the maximum temperature lift between the two solid pieces was around 7 K. A similar result of 7 K was achieved by a much simpler design using a motive Ni-Ti ribbon under indirect tension force (Ossmer et al. 2015). The heat transfer mechanism was also realized by using the contact between SMA bed and solid-pieces without a HTF.

The scope of this study is an extension of previous works by Qian et al. (2015b) to further demonstrate the capability of the single stage cycle design with larger cooling capacity. By scaling up the previous design's capacity with more Ni-Ti tubes and more HTF flow rate, a better system performance is expected due to the reduction of the ratio between the heat losses and the useful cooling power generated by SMA materials in this prototype.

Driving subsystem

The previous system layout designed by Qian et al. (2015b) was followed and extended in this study, as illustrated by Figure 2. Ni-Ti tubes purchased from Nitinol Devices and Components (NDC) Inc. were mounted in four SMA beds. Since a holder was used to prevent tubes from buckling during axial compression in each bed, two linear bearings were used to align them. Two SMA beds were located on the top and another two beds on the bottom. This symmetric design enabled the work recovery feature to improve system efficiency, which means that both the top and bottom SMA beds were set to 50% maximum strain under equilibrium condition. When the top two SMA beds were unloaded from 100% maximum strain back to the equilibrium strain, the unloading force could be used to automatically load the bottom two SMA beds without using the driver. From the equilibrium strain state to the strain-free state, the force provided by the driver could be reduced due to the remaining stress from the top two SMA beds. The two sets of drivers in Figure 2 were located in the middle of the two SMA beds in order to balance the force distribution along the intermediate moving plate. Two sets of rail guides were implemented to align and guide the vertical movement of the plate. The frame balanced the force between the two drivers and the four SMA beds.

To compress more Ni-Ti tubes in this prototype, the hydraulic system was chosen as a driver instead of the mechanical linear actuator used in the previous prototype (Qian et al. 2015b). Compared with the mechanical linear actua-

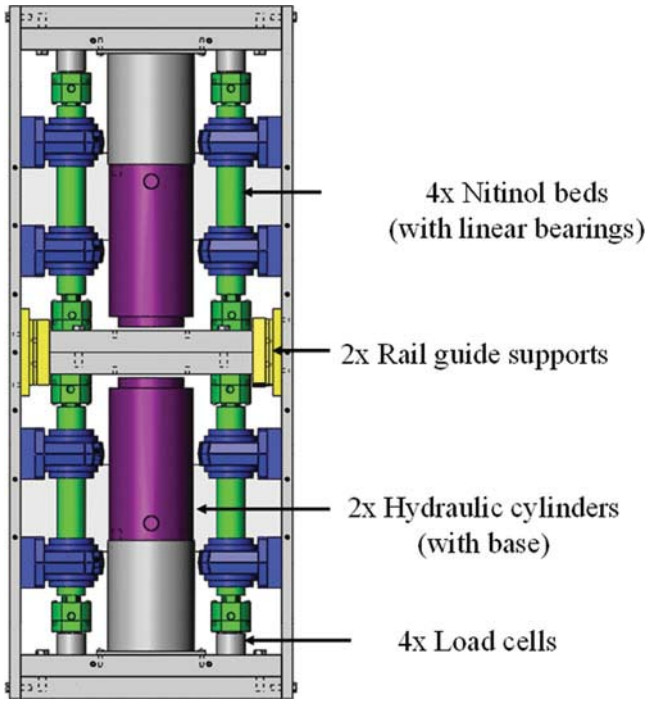

Fig. 2. Illustration of the driving mechanism and system layout.

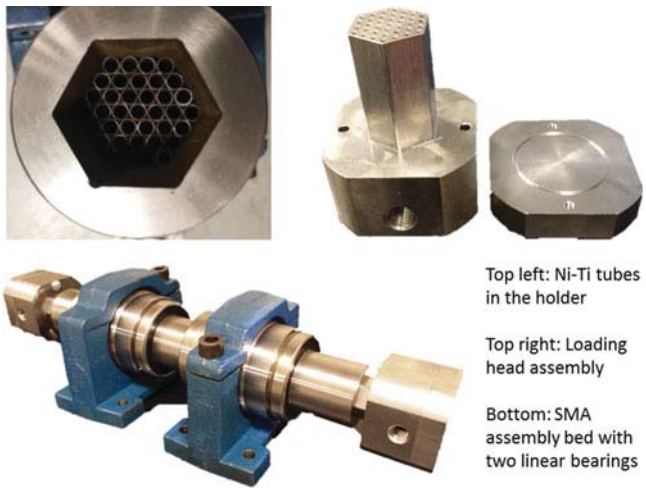

Fig. 3. Photo of the SMA bed in the prototype.

tor, the hydraulic cylinder is not only more powerful, but is also much more compact. The only drawback is that most of the hydraulic cylinders can only provide pushing force when charged with hydraulic oil, which means that either two hydraulic cylinders arranged in the opposite direction or a more complicated two-way cylinder is required. In the current work, two identical one-way hydraulic cylinders with 100 cm^2 working area were implemented along the same axis in opposite direction. Therefore, the bottom hydraulic cylinder in Figure 2 was charged when the top two SMA beds were compressed, and vice versa. They were designed to operate under pressures up to 689 bar, which is equivalent to the maximum force of 689 kN.

Figure 3 is a photo of the details in a SMA bed with Ni-Ti tubes inside. The Ni-Ti tubes were bounded by the holder and compressed axially by two sets of loading head assembly, which were used to distribute the HTF uniformly into each Ni-Ti tube and transfer the large compressive force. The entire bed assembly was aligned by two linear bearings. More detailed geometry information regarding the bed, frame and cylinder in the prototype can be found in Table 1. The uniaxial stress was calculated from force measurement by load cells and cross-sectional area of the Ni-Ti tubes measured by micrometer, which resulted in an overall uncertainty of around 2%. The strain was calculated by a displacement sensor's reading and the overall length of the Ni-Ti tubes, which corresponded to 1% overall uncertainty.

Heat transfer subsystem

The driver subsystem introduced in the last section determines the loading and unloading process illustrated in Figure 1. The rest of the cycle requires involvement of heat transfer from the SMA beds, including the heat rejection/absorption and HR processes, which are based on cyclically flowing the corresponding HTF into those SMA beds. Water was chosen as the HTF for its convenience. Figure 4 is a schematic of the HTF subsystem. Both the top and the bottom two SMA beds were connected by HTF in parallel. There were three loops, including a heat rejection loop, a heat absorption loop, and a HR loop. These three separate loops were merged to four HTF distributors before being connected to the four SMA beds. The cyclical HTF flow was achieved by cyclical control of 10 solenoid valves in the previously mentioned three separate HTF loops. Three pumps, including a variable speed pump for the HR loop, were implemented to drive the HTF flow in their specific loop. The variable speed feature for the HR pump was to optimize the HR flow rate during system operation based on the method proposed by Qian et al. (2015c). Tube-fin heat exchangers were used as the heat sink and heat source, wherein hot air and cold air were blowing out of the heat sink and heat source, respectively. Those sensors used in the test rig are also shown in Figure 5, including two Coriolis mass flow meters with 0.1 g/s uncertainty under 100 g/s mass flow rate, sixteen T type thermocouples calibrated with 0.2 K uncertainty between 0°C to 50°C, and two differential pressure transducers with 0.5 kPa uncertainty.

Two novel designs were applied from the literature (Qian et al. 2015d). As illustrated in Figure 5a, the first design was to add plastic inserts inside each Ni-Ti tube to reduce the dead thermal mass of the HTF and the associated cyclic loss. ABS plastic insertions made by the adhesive manufacturing technique (a.k.a. 3-D printing) were implemented in each Ni-Ti tube, which blocked approximately 50% of the flow cross-sectional area, and reduced around 35% of the total dead thermal mass. The reduction in the cross-section area corresponded to around a 20% pressure drop increase, which was a tradeoff for this design. The second novel design approach applied in the prototype was the plastic insulation tube design. Those plastic insulation tubes inside the loading head, between each Ni-Ti tube to the external HTF pipe, reduced the heat loss from the HTF to the metal loading head significantly. A graphic illustration of the plastic insulation tube concept is also shown in Figure 5b.

Table 1. Key parameters of the prototype.

Ni-Ti tube quantity	19 (ea per bed)	Frame height	1219.2 (mm)
Ni-Ti tube inner diameter	3.76 (mm)	Frame width	152.4 (mm)
Ni-Ti tube outer diameter	4.72 (mm)	Frame length	609.6 (mm)
Ni-Ti tube length	254 (mm)	Frame thickness	19.1 (mm)
Ni-Ti tube weight	10.6 (g)	Hydraulic cylinder area	10,060 (mm^2)
Bed holder diameter	50.8 (mm)	Hydraulic cylinder height	279.4 (mm)
Bed holder length	330.2 (mm)	Cylinder base height	304.8 (mm)
Loading head length	101.6 (mm)		

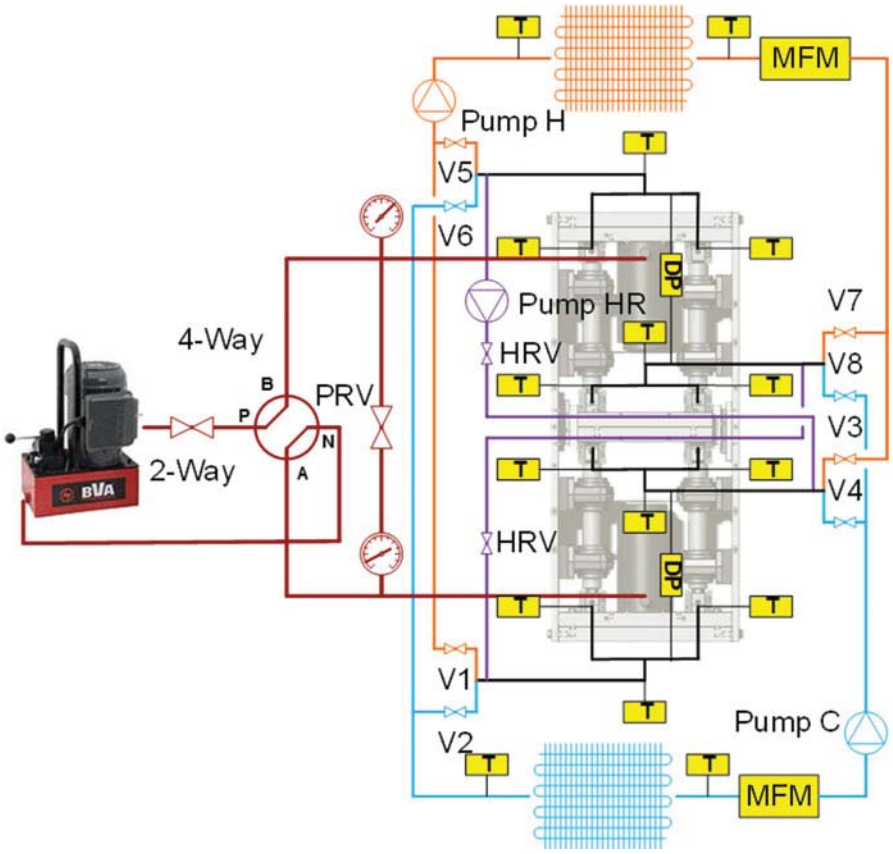

Fig. 4. Schematic of the heat transfer fluid subsystem with hydraulic fluid loop.

Performance demonstration

A preliminary test was carried out to confirm the material's latent heat in the system under compression mode. Upon loading, heat was rejected from the Ni-Ti tubes to the flowing HTF inside them, generating a temperature spike at the outlet of the bed. By integrating the temperature difference between the inlet and outlet water, and applying water mass flow rate as a multiplier, the accumulated heat carried by the water (Q) could be used to estimate the material's latent heat, assuming all heat losses were negligible. This method is described by Eq. (1), where m is the instantaneous mass flow rate, c_{p} is the specific heat of water, and $T_{\mathrm{f,out}}$ and $T_{\mathrm{f,\,in}}$ are the outlet and inlet water temperature, respectively. The loading speed was 10 s for each strain. Since Eq. (1) integrated the heat over the entire loading process, the result was independent of the loading speed.

$$Q = c_p \int_0^t \dot{m}\left(T_{f,out} - T_{f,in}\right) dt \tag{1}$$

The test was conducted multiple times under each strain. Figure 6 presents the test results under various compressive strains. The expected latent heat from the material based on literature (Cui et al., 2012) was $10 \sim 12\ \mathrm{J{\cdot}g^{-1}}$, which was achieved in this prototype under 4.5% strain. The maximum loading and unloading latent heat achieved under 4.5% strain were 11.7 and $10.4\ \mathrm{J{\cdot}g^{-1}}$, respectively.

There are a few indices to evaluate a system's performance. The system temperature lift (ΔT_{lift}) is defined as the water temperature difference between the heat sink and the heat source, as shown in Eq. (2). It is the temperature difference between two streams of fluid, if HTF is used, or between two solids if there is no HTF (Ossmer et al. 2015; Schmidt et al. 2015). It evaluates the application potential of this specific cooling technology, as a small temperature lift is only capable to satisfy the need of very limited applications. The coefficient of performance (COP) defined in Eq. (3) measures the energy conversion efficiency, wherein the numerator is the cooling capacity and the denominator is the overall power consumption, including both the hydraulic driver's power and the parasitic power consumption by valves and pumps.

$$\Delta T_{lift} = T_{f,sink} - T_{f,source} \tag{2}$$

$$COP = Q_c/(W + W_{parasitic}) \tag{3}$$

To increase the system COP, a previous study by Qian et al. (2015a) suggested isothermal loading instead of adiabatic loading as shown in Figure 1, to minimize the so-called adiabatic loss. The physical reason behind this loss was due to additional stress and energy required to load the material during adiabatic phase changes and temperature increase of the material. To quantitatively validate the COP increasing potential by substituting adiabatic loading with isothermal loading, a series of tests were conducted to compare the

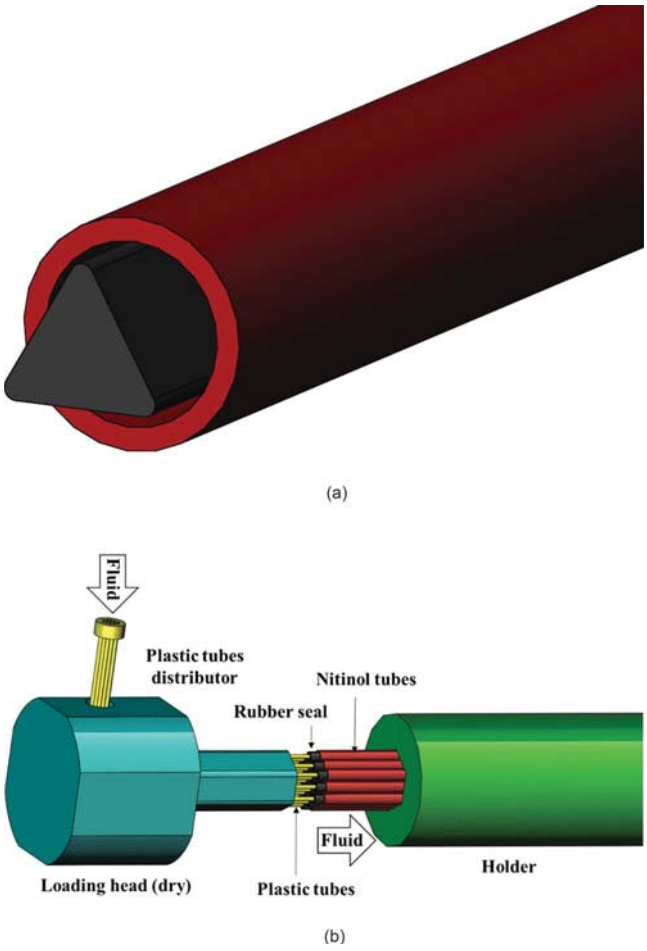

Fig. 5. Illustrations of the plastic insertion and the plastic insulation tube designs.

enclosed area of the loading–unloading curve on the stress–strain diagram. Without any water flow, the loading speed was varied from 0.1 to 1500 s to achieve different heat transfer conditions from the adiabatic limit to the isothermal limit. For example, the loading speed in the previous prototype was between 0.1 to 1 s (Qian et al. 2015b) without water flow, which was close to the adiabatic limit since no heat could be dissipated to the HTF within that short duration. The 1500 s loading speed corresponded to the isothermal limit when the recorded temperature change of the material was less than 1 K during the loading process. The difference between the adiabatic and isothermal limits can be visualized in Figure 7. The enclosed area of each loading-unloading curve in Figure 7 is directly proportional to the driver's power term W in Eq. (2). The corresponding specific work ranged from 2.2 to 2.4 $J \cdot g^{-1}$ between 0.1 to 1 s loading speed. It was reduced to 1.5 $J \cdot g^{-1}$ under 50 s loading speed, and eventually dropped to 1.1 $J \cdot g^{-1}$ after 500 s loading speed. In Figure 7, the stress became negative under fast loading/unloading scenarios. This phenomenon was because the unloading phase change took longer time than the unloading process, as discussed by Tusek et al. (2015b). During the test, the tubes were idled for 15 s each time after loading and unloading to allow full phase transformation. In the prototype developed in this study, the hydraulic cylinder was capable to fully load the Ni-Ti tubes within 6 $\sim$ 10 s depending on the hydraulic pressure. This 6 s loading with HTF flowing was equivalent to at least 50 s loading without HTF. Therefore, this preliminary result in Figure 7 indicates theoretically that the work required to drive the system can be reduced more than 50% by switching from adiabatic loading to isothermal loading. In practice, if partial of the unloading energy cannot be fully harvested, 30% reduction is a conservative estimation of the COP improvement.

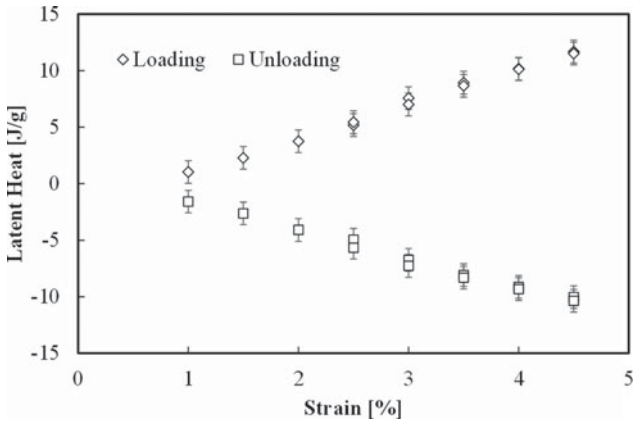

Fig. 6. Preliminary measurement of the material's latent heat in the prototype.

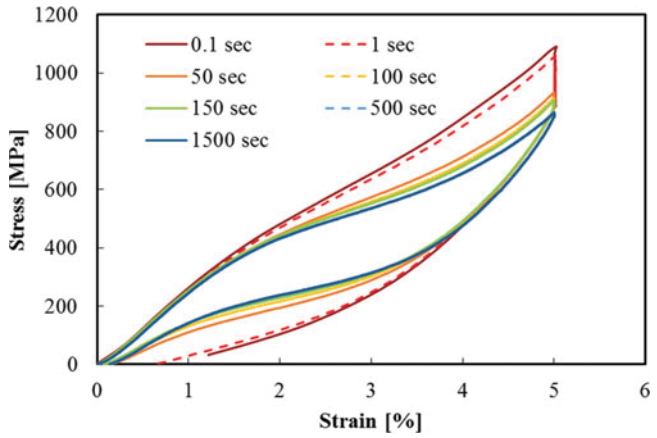

Fig. 7. Preliminary loading and unloading stress–strain hysteresis measurement in the prototype.

With the benefit of approaching the isothermal loading, Figure 8 presents the predicted system performance by using a previous dynamic system model (Qian et al. 2015a). More tests will be conducted in the future to validate this prediction. The model was based on 1D energy equations, which coupled the HTF and Ni-Ti temperature variations together. The heat transfer between the HTF and Ni-Ti tubes, the complicated HTF flow inside the HTF network, as well as the phase transformation of Ni-Ti tubes were solved simultaneously. In the model, 10 $J \cdot g^{-1}$ latent heat was assumed when the Ni-Ti tubes were under 5% compressive strain. Since the energy equations

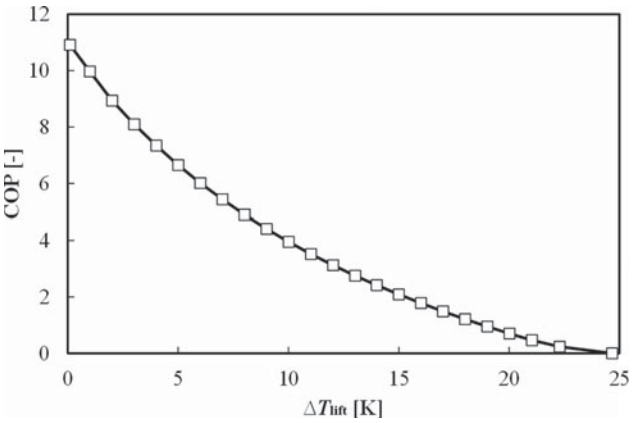

Fig. 8. Predicated performance map based on a previously developed dynamic model (heat source water temperature $T_c = 20 - 0.5\Delta T_{lift}$, heat sink water temperature $T_h = 20 + 0.5\Delta T_{lift}$).

were solved simultaneously, the temperature variations of the Ni-Ti tubes were determined based on the loading strain rate and the HTF flow rate. As a result, the maximum temperature variations of the Ni-Ti tubes determine the real work required to drive the cycle. Since the model was purely based on physical heat transfer processes, there is no explicit assumption to determine whether the Ni-Ti tubes were undergoing "isothermal" or "adiabatic" phase changing. It means that the Ni-Ti tubes are neither "adiabatic" nor "isothermal." In fact, typical temperature variations during loading/unloading were less than 5 K under 6 ~ 10 s loading rate and HTF flow, whereas the material itself has an adiabatic temperature span of almost 20 K. The 5 K temperature variation limits the heat transfer rate to the HTF, which is the major tradeoff between enhancing COP and cooling capacity. The COP in Figure 8 also included the pumps' power consumption, which was 5.9 W based on pressure drop and the volumetric flow rate of the HTF under 0.8 $m{\cdot}s^{-1}$ fluid velocity across each Ni-Ti tube during heat transfer and 0.2 $m{\cdot}s^{-1}$ velocity during HR. When considering both the plastic insulation and tube insertions, the cooling capacity under 10 K system temperature lift was 139 W. The COP in Figure 8 measures the overall system energy conversion efficiency based on Eq. (3), which is different from the material COP. In fact, one may determine the material COP of 12.1 by the latent heat from Figure 6 and the net loading energy of the material from Figure 7. The maximum system COP achieved was 11.0 and the maximum system temperature lift for this single-stage system was 24.6 K. Compared with the first mechanical driven prototype (Qian et al. 2015b), which was designed with the maximum system temperature lift of 16 K, the hydraulic driven prototype reduced the dead thermal mass per unit active Ni-Ti material mass, and therefore, achieved 8.6 K more system temperature lift. In addition, the maximum system temperature lift was even higher than the adiabatic temperature span (ΔT_{ad}) of the Ni-Ti tube, which was defined as the measured temperature change during an adiabatic loading process. This means that HR played an important role to boost the system performance. In fact, the HR efficiency achieved under the design condition in Figure 8 was around 57%. Optimizing the flow velocity, duration and better tuning the HR HTF pipe length and diameter in the future could lead to further improvements in the prototype's performance.

Conclusions

In this study, a new design of a hydraulically driven compressive elastocaloric cooling system using Ni-Ti tubes was demonstrated. The compact hydraulic cylinder was capable of compressing enough Ni-Ti tubes in order to provide hundreds of Watts of cooling. Two novel designs introduced in the literature have been applied to the prototype, including the plastic insertion to minimize the dead thermal mass of fluid and plastic insulation tube to minimize heat losses. By using the water flow rate and temperature difference method, preliminary tests were conducted and results indicated that the Ni-Ti tube could provide latent heat of more than 10 $J{\cdot}g^{-1}$ under 4.5% strain. The hydraulic cylinder operated under 6 ~ 10 s loading speed also enabled more than 30% power reduction of the driver by approaching the isothermal loading limit. Based on a previously developed system model, the maximum water-to-water system temperature lift could be 24.6 K, and the maximum system COP could be 11.0. The system COP of 3.9 under 10 K temperature lift corresponded to 14% of the Carnot cycle COP under the same temperatures. More comprehensive system performance testing will be conducted in the future.

Nomenclature

COP	= coefficient of performance
c_p	= specific heat ($J{\cdot}g^{-1}{\cdot}K^{-1}$)
HR	= heat recovery
HTF	= heat transfer fluid
$\dot{m}$	= mass flow rate ($g{\cdot}s^{-1}$)
Q	= capacity (W)
SMA	= shape memory alloys
s	= specific entropy ($J{\cdot}g^{-1}{\cdot}K^{-1}$)
t	= time (sec)
T_c	= heat source temperature (°C)
$T_{f,\,in}$	= inlet water temperature (°C)
$T_{f,out}$	= outlet water temperature (°C)
T_h	= heat sink temperature (°C)
ΔT_{ad}	= adiabatic temperature span (K)
ΔT_{lift}	= system temperature lift (K)
W	= power consumption (W)
ε	= strain (–)
σ	= stress (MPa)

Acknowledgments

The authors would like to thank Dr. Jun Cui, Dr. Yiming Wu, and PNNL for their professional assistance.

Funding

The authors gratefully acknowledge the support of this effort from the U.S. DOE (ARPA-E DEAR0000131) and the Center for Environmental Energy Engineering (CEEE) at the University of Maryland.

References

Cui, J., Y. Wu, J. Muehlbauer, Y. Hwang, R. Radermacher, S. Fackler, M. Wuttig, and I. Takeuchi. 2012. Demonstration of high efficiency elastocaloric cooling with large Delta T using NiTi wires. *Applied Physics Letters* 101(7):073904. DOI:10.1063/1.4746257

Jacobs, S., J. Auringer, A. Boeder, J. Chell, L. Komorowski, J. Leonard, S. Russek, and C. Zimm. 2014. The performance of a large-scale rotary magnetic refrigerator. *International Journal of Refrigeration* 37(1):84–91.

Kitanovski, A., U. Plaznik, U. Tomc, and A. Poredos. 2015. Present and future caloric refrigeration and heat pump technologies. *International Journal of Refrigeration* 57:288–98.

Manosa, L., A. Planes, and E. Vives. 2009. The use of shape-memory alloys for mechanical refrigeration. *Functional Materials Letters* 2(2):73–8.

Ossmer, H., S. Miyazaki, and M. Kohl. 2015. *Elastocaloric Heat Pumping Using a Shape Memory Alloy Foil Device*. Anchorage, AK: TRANSDUCERS. DOI:10.1109/TRANSDUCERS.2015.7181026.

Otsuka, K., and C.K. Wayman. 1998. *Shape Memory Materials*. London, UK: Cambridge University Press.

Ozbolt, M., A. Kitanovski, J. Tusek, and A. Poredos. 2014. Electrocaloric refrigeration: Thermodynamics, state of the art and future perspectives. *International Journal of Refrigeration* 40:174–88.

Qian, S., Y. Geng, Y. Wang, J. Ling, Y. Hwang, R. Radermacher, I. Takeuchi, and J. Cui. 2016a. A review of elastocaloric cooling: materials, cycles, and system integration. *International Journal of Refrigeration* 62:1–19.

Qian, S., D. Nasuta, A. Rhoads, Y. Wang, Y. Geng, Y. Hwang, R. Radermacher, and I. Takeuchi. 2016b. Not-in-kind cooling technologies: A quantitative comparison of refrigerants and system performance. *International Journal of Refrigeration* 62:177–92.

Qian, S., J. Ling, Y. Hwang, R. Radermacher, and I. Takeuchi. 2015a. Thermodynamic cycle analysis and numerical modeling of thermoelastic cooling systems. *International Journal of Refrigeration* 56:65–80.

Qian, S., Y. Wu, J. Ling, J. Muehlbauer, Y. Hwang, I. Takeuchi, and R. Radermacher. 2015b. Design, development and testing of a compressive thermoelastic cooling prototype. *International Congress of Refrigeration*, Japan. Paper 0092.

Qian, S., J. Ling, J. Muehlbauer, Y. Hwang, and R. Radermacher. 2015c. Study on high efficient heat recovery cycle for solid-state cooling. *International Journal of Refrigeration* 55:102–19.

Qian, S., A. Alabdulkarem, J. Ling, J. Muehlbauer, Y. Hwang, R. Radermacher, and I. Takeuchi. 2015d. Performance enhancement of a compressive thermoelastic cooling system using multi-objective optimization and novel designs. *International Journal of Refrigeration* 57:62–76.

Schmidt, M., A. Schutze, and S. Seelecke. 2014. Experimental investigation on the efficiency of a control dependent NiTi-based cooling process. *Proceedings of the ASME SMASIS, Newport, RI*, September 8–10.

Schmidt, M., A. Schutze, and S. Seelecke. 2015. Scientific test setup for investigation of shape memory alloy based elastocaloric cooling processes. *International Journal of Refrigeration* 54:88–97.

Tusek, J., K. Engelbrecht, R.M. Solsona, L. Manosa, E. Vives, L.P. Mikkelsen, and N. Pryds 2015a. The elastocaloric effect: A way to cool efficiently. *Advanced Energy Materials* 5(13):1500361. DOI:10.1002/aenm.201500361

Tusek, J., K. Engelbrecht, L.P. Mikkelsen, and N. Pryds. 2015b. Elastocaloric effect of Ni-Ti wire for application in a cooling device. *Journal of Applied Physics* 177(12):124901. DOI:10.1063/1.4913878